Supplementary Information

The Exploration of a New Stable G-Triplex DNA and Its Novel Function in Electrochemical Biosensing

Ling-Li Zhao[a], Ting Cao[a], Qian-Yu Zhou[a], Xiao-Hui Zhang[a,b], Ying-Lin Zhou[a,*], Lijiang Yang[a,*], Xin-Xiang Zhang[a]

[a.] Beijing National Laboratory for Molecular Sciences (BNLMS), MOE Key Laboratory of Bioorganic Chemistry and Molecular Engineering, College of Chemistry and Molecular Engineering, Peking University, Beijing 100871, China. [b.] State Key Laboratory of Natural and Biomimetic Drugs, Peking University, 38 Xueyuan Road, Beijing 100191, China.

*E-mail: zhouyl@pku.edu.cn. Correspondence may also be addressed to Lijiang Yang, E-mail: yanglj@pku.edu.cn.

Table of Content

The calculation of the surface area of the ultramicroelectrode S-3

Binding analysis-MS strategy for determination of binding constants S-4

Table S1. DNA sequences used in this work S-5

Table S2. Compositions of the simulation systems S-6

Table S3. Guanine glycosidic angles variations of G4/G3 along 600 ns MD trajectories S-7

Table S4. Guanine glycosidic angles variations of G4 with MB along 200 ns MD trajectories S-8

Table S5. Guanine glycosidic angles variations of G3 with MB along 200 ns MD trajectories S-9

Table S6. The binding free energies (kcal mol^{-1}) of MB obtained from MM/PBSA calculations. S-10

Table S7. The overlapping area ($Å^2$) of MB and bases S-11

Table S8. Comparison of different aptasenors for the determination of cocaine S-12

Table S9. Cocaine detection spiked with 20% human urine via CocG3 strategy (n=3). S-13

Figure S1. The CV of carbon fiber ultramicroelectrode inserted in the micropipette with 20 μL solution containing 5 mM $K_4Fe(CN)_6/K_3Fe(CN)_6$, scan rate: 0.1 V/s. S-14

Figure S2. SWVs of 10 μM MB in the presence of different concentrations of G3 from a to h: 0, 5, 10, 20, 30, 50, 70, 80 μM, respectively. S-15

Figure S3. Scatchard plot of G3-MB complex. S-16

Figure S4. Standard curve of MB S-17

Figure S5. Fitting curves of (A) G3/MB complex and (B) G4/MB complex S-18

Figure S6. Initial structures of MD simulations: (A) G4 with MB located on the 3' end of G-quartet surface, (B) G4 with MB located on the 5' end surface, (C) G3 with MB located on the 3' end surface and (D) G3 with MB located on the 5' end surface. S-19

Figure S7. Snapshots of (A) G4/MB (3') (B) G4/MB (5') after 200 ns of MD simulations. S-20

Figure S8. SWVs of 2 μM CocG3 and 5 μM MB which were incubated with buffer (black), 1 mM morphine (red), 1 mM atropine (blue), and 1 mM cocaine (green) for 30 min. S-21

Figure S9. The optimization of the concentration of CocG3. The percentage of current reduction $\Delta i/i_0 \times 100\%$ ($\Delta i = i_0 - i_t$), where i_0 and i_t are the currents of the sample in the absence and presence of cocaine, respectively. Experimental conditions: the concentration of MB was fixed to be 5 μM. Error bars: SD, n=3. S-22

Figure S10. The optimization of the concentration of MB. Experimental conditions: the concentration of CocG3 was fixed to be 2 μM. Error bars: SD, n=3. S-23

Figure S11. SWVs of 2 μM CocG3 and 5 μM MB incubated with 0.5 (black), 10 μM (red) and 1 mM (blue) cocaine recorded every 24 h interval S-24

Figure S12. SWVs of 6 replicates of samples containing 2 μM CocG3 and 5 μM MB incubated with 0.5 (black), 10 μM (red) and 1 mM (blue) cocaine S-25

The calculation of the surface area of the ultramicroelectrode

The surface area of the ultramicroelectrode in the experimental section was calculated from the CV of ultramicroelectrode in the 5 mM $K_4Fe(CN)_6/K_3Fe(CN)_6$ solution (Figure S1) and the related calculation of surface area is shown below.

According to the formula[1]: $i_{ss} = 2nFAD_0C_0^*/r_0 \ln\tau$

$i_{ss} = 0.92\times10^{-7}$A

n=1

F= 96485 C/mol

$D_0 = 0.65 \times10^{-5}$ $cm^2/s = 6.5\times10^{-10}$ m^2/s

$C_0^* = 5\times10^{-3}$mol/L =5 mol/m^3

$r_0 = 3.5\times10^{-6}$ m

If t = 3s,

$\tau = 4 D_0 t/ r_0^2 = 637$

$\ln\tau = 6.46$

The surface area of carbon fiber ultramicroelectrode was calculated to be $A = 3.3\times10^{-9}$ m^2.

Binding analysis-MS strategy for determination of binding constants

The binding constants of DNA-MB complexes were determined by an improved mass spectrometric titration methodology, which was based only on the peak intensities of equilibrium DNA and a MB standard curve. A series of samples with a constant concentration of DNA (20 μM) and an increasing concentration of MB from 0.4 to 20 μM were mixed. Considering a 1:1 system (DNA-MB), the binding constant K_a can be calculated as follows:

$$K_a = \frac{[C]}{[D][MB]} \quad (1)$$

where $[C]$, $[D]$ and $[MB]$ are the equilibrium concentrations of DNA-MB complex, DNA and MB, respectively. Ion intensity is positively correlated with concentration but different species have different ionization efficiency. Therefore, ionization efficiency coefficient R is introduced into the calculation. R is defined as follows: R=I/c (I and c are the ion intensity and concentration of the analyte, respectively). Eq 1 can be thus rewritten as:

$$K_a = \frac{\frac{I_0 - I_i}{R}}{\frac{I_i}{R}[MB]} = \frac{I_0 - I_i}{I_i[MB]} \quad (2)$$

Where I_0 and I_i are ion intensity of DNA in the absence of MB and in the presence of different concentration of MB, respectively. Eq 2 can be converted into eq 3 by taking the reciprocal.

$$\frac{1}{I_i} = \frac{K_a}{I_0}[MB] + \frac{1}{I_0} \quad (3)$$

Finally, we can obtain the binding constants based on the concentration of MB, the ion intensity in the absence of MB and in the presence of different concentration of MB. The concentration of MB is obtained by pre-determined standard curve of MB (Figure S4) and measured ion intensity of MB. The binding constant for each complex was obtained from the slope of a weighted least-squares regression fit of the data to eq 3 (Figure S5).

Table S1. DNA sequences used in this work

Name	Sequence (5' to 3')
G3	CTGGGAGGGAGGGA
G4	CTGGGAGGGAGGGAGGGA
Truncated G4-10	CTGGGAGGGA
Truncated G4-11	CTGGGAGGGAG
Truncated G4-12	CTGGGAGGGAGG
Truncated G4-13	CTGGGAGGGAGGG
Truncated G4-15	CTGGGAGGGAGGGAG
Truncated G4-16	CTGGGAGGGAGGGAGG
Truncated G4-17	CTGGGAGGGAGGGAGGG
C3	TCCCTCCCTCCCAG
CocG3	CTGGGAGGGAGGGATGTCGAGGGAGACAAGGAAAATCCTTCAAT GAAGTGGGTCGACATCCC
CocG4	CTGGGAGGGAGGGAGGGATGTCGAGGGAGACAAGGAAAATCCT TCAATGAAGTGGGTCGACATCCC

Table S2. Compositions of the simulation systems

DNA	Initial MB Pos	# H_2O	# K^+	# Cl^-	System ID
G4	N/A	4416	34	17	G4
G3	N/A	3874	26	13	G3
G4	3' end	5034	34	17	G4-3'
	5' end	5242			G4-5'
G3	3' end	4510	26	13	G3-3'
	5' end	4050			G3-5'

Table S3. Guanine glycosidic angles variations of G4/G3 along 600 ns MD trajectories

Base	Avg (º) G4	Std (º) G4	Avg(º) G3	Std (º) G3
DG3	-85.60	13.49	-96.29	15.93
DG4	-123.01	28.07	-99.08	11.77
DG5	-115.18	14.43	-98.29	14.33
DG7	-141.65	25.56	-105.89	15.25
DG8	-105.26	17.01	-100.21	16.29
DG9	-124.13	23.74	-100.06	16.26
DG11	-136.94	19.16	-102.11	26.38
DG12	-97.81	12.47	-112.57	30.98
DG13	-125.72	21.71	-98.19	17.68
DG15	-144.05	19.51	N/A	N/A
DG16	-89.85	12.00	N/A	N/A
DG17	-116.60	12.37	N/A	N/A

Table S4. Guanine glycosidic angles variations of G4 with MB along 200 ns MD trajectories

Base	Avg (º) G4-3'	Std (º) G4-3'	Avg(º) G4-5'	Std (º) G4-5'
DG3	-93.3864	17.46	-107.53	22.20
DG4	-110.67	18.01	-126.86	37.66
DG5	-119.07	13.79	-113.56	14.28
DG7	-141.45	19.45	-135.03	25.59
DG8	-100.32	14.34	-106.42	15.86
DG9	-116.98	12.80	-119.00	14.83
DG11	-135.45	23.86	-137.53	26.24
DG12	-105.46	14.10	-104.09	15.29
DG13	-116.68	13.84	-118.96	12.60
DG15	-130.14	25.63	-140.56	23.35
DG16	-103.30	27.09	-103.63	22.41
DG17	-109.45	14.01	-113.54	14.01

Table S5. Guanine glycosidic angles variations of G3 with MB along 200 ns MD trajectories

Base	Avg (º) G3-3'	Std (º) G3-3'	Avg(º) G3-5'	Std (º) G3-5'
DG3	-106.02	15.46	-91.65	16.56
DG4	-100.02	12.36	-94.09	11.63
DG5	-102.74	14.58	-127.75	29.50
DG7	-119.58	19.19	-116.75	21.24
DG8	-111.15	17.81	-99.08	16.13
DG9	-123.86	16.61	-105.71	14.59
DG11	-127.36	21.01	-124.76	55.90
DG12	-95.56	18.51	-103.43	14.36
DG13	-109.14	14.72	-85.37	16.08

Table S6. The binding free energies (kcal mol^{-1}) of MB obtained from MM/PBSA calculations.

DNA	ΔG (3')	ΔG (5')
G4	-1.09±3.73	-7.32±4.28
G3	-16.44±4.77	-20.33±4.37

Table S7. The overlapping area (Å^2) of MB and bases

DNA	Area (3')	Area (5')
G4	59.2	61.6
G3	76.1	77.4

Table S8. Comparison of different aptasenors for the determination of cocaine

Analytical method	Signal transduction	Dynamic range	Detection limit
This work	Electrochemistry	500 nM-1000 μM	500 nM
G-quadruplex probe for electrochemical biosensing[2]	Electrochemistry	5 μM-1000 μM	5 μM
Heterogeneous electrochemical aptasensor[3]	Electrochemistry	10-2000 μM	Below10 μM
Aptamer-Based Folding Fluorescent Sensor[4]	Fluorescence	10-4000 μM	10 μM
Single-quantum dot-based aptametic sensor[5]	Fluorescence resonance energy transfer	500 nM-10 μM	500 nM
Sensor design involving aptamers and nanoparticles[6]	Colorimetry	50-500 μM	50 μM
Biological nanopore embedded in a microchip[7]	Biological nanopore	1 μM-100 μM	1 μM

Table S9. Cocaine detection spiked with 20% human urine via CocG3 strategy (n=3).

$c_{(cocaine)}$	Δi (Without spiking)/nA	Δi (Spiked with 20% human urine)/nA	Recovery
10 μM	62.2 (±0.8)	67.1 (±2.0)	108%
100 μM	87.2 (±1.0)	82.1 (±1.8)	94.2%

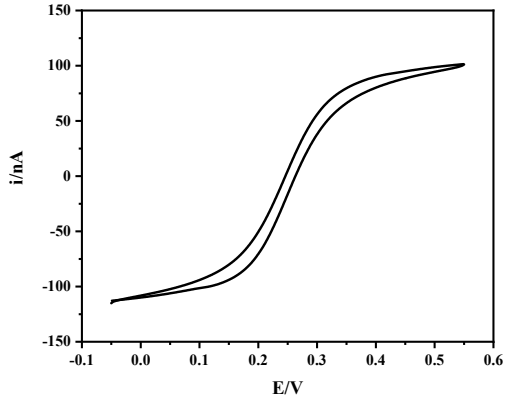

Figure S1. The CV of carbon fiber ultramicroelectrode inserted in the micropipette with 20 μL solution containing 5 mM $K_4Fe(CN)_6/K_3Fe(CN)_6$, scan rate: 0.1 V/s.

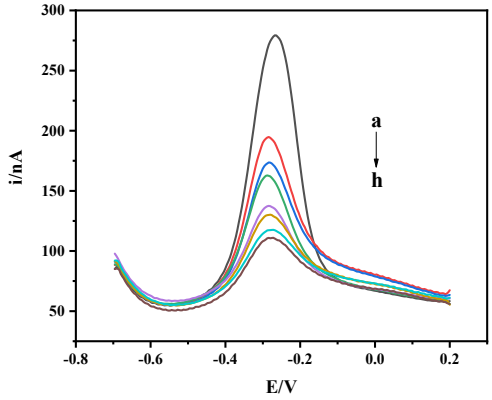

Figure S2. SWVs of 10 μM MB in the presence of different concentrations of G3 from a to h: 0, 5, 10, 20, 30, 50, 70, 80 μM, respectively.

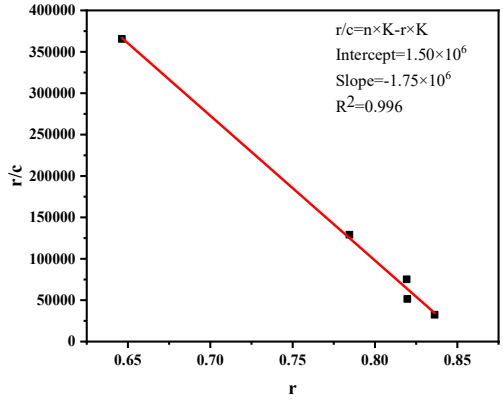

Figure S3. Scatchard plot of G3-MB complex.

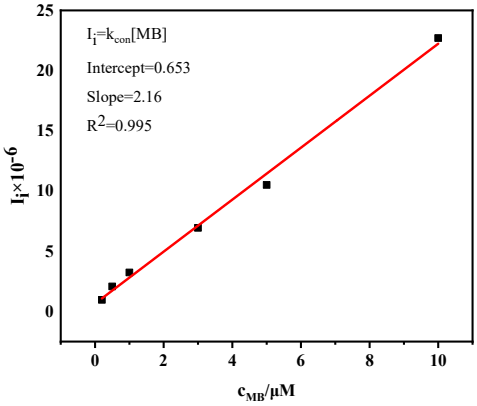

Figure S4. Standard curve of MB

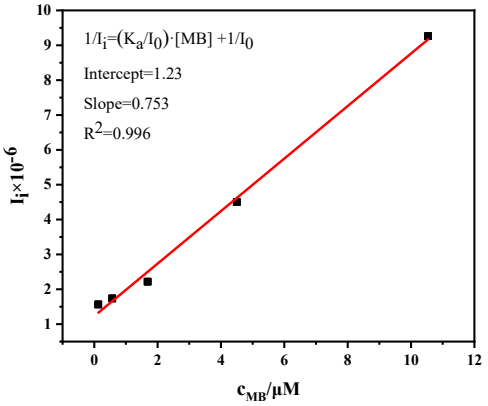

(A)

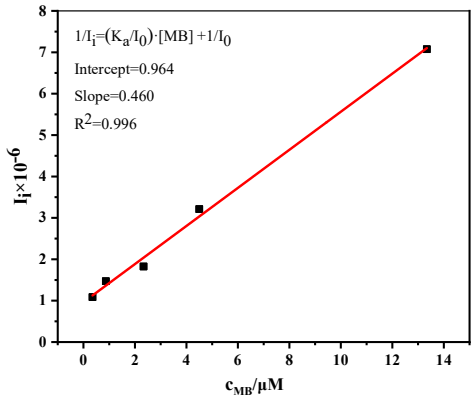

(B)

Figure S5. Fitting curves of (A) G3/MB complex and (B) G4/MB complex

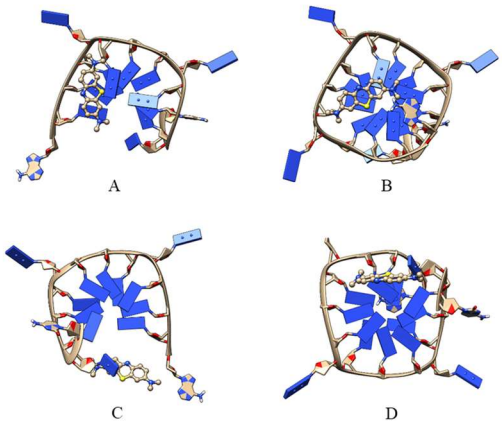

Figure S6. Initial structures of MD simulations: (A) G4 with MB located on the 3' end of G-quartet surface, (B) G4 with MB located on the 5' end surface, (C) G3 with MB located on the 3' end surface and (D) G3 with MB located on the 5' end surface.

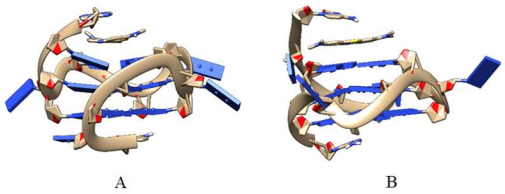

Figure S7. Snapshots of (A) G4/MB (3') (B) G4/MB (5') after 200 ns of MD simulations.

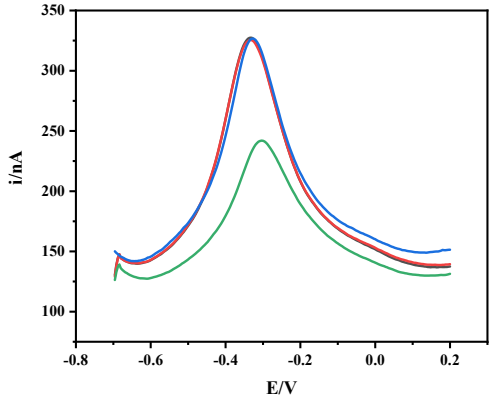

Figure S8. SWVs of 2 μM CocG3 and 5 μM MB which were incubated with buffer (black), 1 mM morphine (red), 1 mM atropine (blue), and 1 mM cocaine (green) for 30 min.

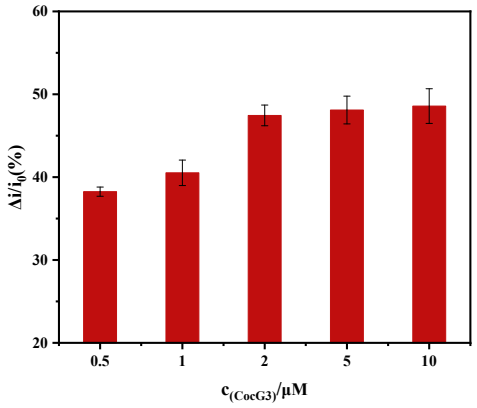

Figure S9. The optimization of the concentration of CocG3. The percentage of current reduction $\Delta i/i_0 \times 100\%$ ($\Delta i = i_0 - i_t$), where i_0 and i_t are the currents of the sample in the absence and presence of cocaine, respectively. Experimental conditions: the concentration of MB was fixed to be 5 μM. Error bars: SD, n=3.

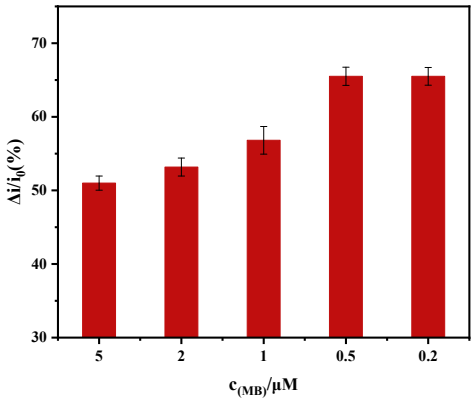

Figure S10. The optimization of the concentration of MB. Experimental conditions: the concentration of CocG3 was fixed to be 2 μM. Error bars: SD, n=3.

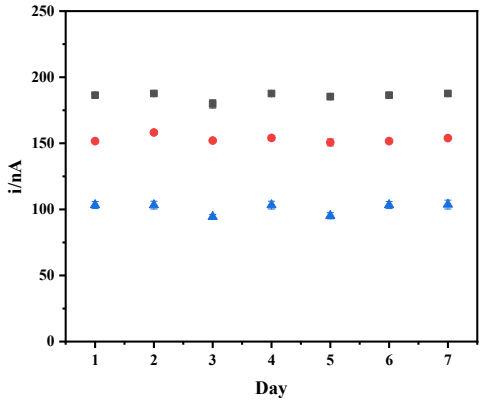

Figure S11. SWVs of 2 μM CocG3 and 5 μM MB incubated with 0.5 (black), 10 μM (red) and 1 mM (blue) cocaine recorded every 24 h interval

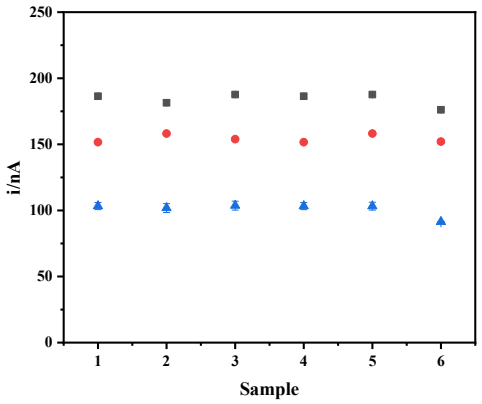

Figure S12. SWVs of 6 replicates of samples containing 2 µM CocG3 and 5 µM MB incubated with 0.5 (black), 10 µM (red) and 1 mM (blue) cocaine

References

1. Bard, A. J.; Faulkner, L. R., *Electrochemical Methods: Fundamentals and Applications*. Wiley: 2000.
2. Zhang, F.-T.; Nie, J.; Zhang, D.-W.; Chen, J.-T.; Zhou, Y.-L.; Zhang, X.-X., Methylene blue as a G-quadruplex binding probe for label-free homogeneous electrochemical biosensing. *Anal. Chem.* **2014,** *86* (19), 9489-9495.
3. Baker, B. R.; Lai, R. Y.; Wood, M. S.; Doctor, E. H.; Heeger, A. J.; Plaxco, K. W., An electronic, aptamer-based small-molecule sensor for the rapid, label-free detection of cocaine in adulterated samples and biological fluids. *J. Am. Chem. Soc.* **2006,** *128* (10), 3138-3139.
4. Stojanovic, M. N.; De Prada, P.; Landry, D. W., Aptamer-based folding fluorescent sensor for cocaine. *J. Am. Chem. Soc.* **2001,** *123* (21), 4928-4931.
5. Zhang, C.-y.; Johnson, L. W., Single quantum-dot-based aptameric nanosensor for cocaine. *Anal. Chem.* **2009,** *81* (8), 3051-3055.
6. Liu, J.; Lu, Y., Fast colorimetric sensing of adenosine and cocaine based on a general sensor design involving aptamers and nanoparticles. *Angew. Chem. Int. Ed.* **2006,** *45* (1), 90-94.
7. Kawano, R.; Osaki, T.; Sasaki, H.; Takinoue, M.; Yoshizawa, S.; Takeuchi, S., Rapid detection of a cocaine-binding aptamer using biological nanopores on a chip. *J. Am. Chem. Soc.* **2011,** *133* (22), 8474-8477.